Novel hermetically sealed device to realize unconventional phonon blockade at near-micron dimensions and milliKelvin temperatures

View Online　　Export Citation　　CrossMark

Jayant K. Nema,[1] **Srijan Gupta,**[2] **Riya Thakkar,**[2] **and Prabhu Rajagopal**[1,a] (iD)

AFFILIATIONS

[1] Centre for Nondestructive Evaluation and Department of Mechanical Engineering, Indian Institute of Technology Madras, Chennai 600036, India

[2] Department of Physics, Indian Institute of Technology Madras, Chennai 600036, India

[a] Author to whom correspondence should be addressed: prajagopal@iitm.ac.in

ABSTRACT

This paper proposes a novel design for a hermetically sealable device, consisting of charged linear and nonlinear membranes driven in the gigahertz range in vacuum setting, as a source of antibunched single phonons. Constraints for effecting phonon antibunching are found using the stationary Liouville–von Neumann master equation. Using analytical calculations and material and geometry optimization, we show that sizes of the proposed system can be upscaled to the near-micrometer range in a trade-off with the system operating temperature. The results are significant to realize quantum phononics, which has much promise as a modality for sensing and computing applications.

I. INTRODUCTION

Phononics is a relatively new branch of science and engineering, encompassing the study and application of various mechanical/elastic wave phenomena (including vibration, acoustics, ultrasonics, hypersonics, and thermal transport). Phonons refer to quantized states of vibration (in analogy to photons that similarly quantify light), which underlie all elastic wave phenomena.[1,2] Today, elastic waves are vital to a range of applications for sensing, imaging, and diagnostics in engineering and biomedicine.[3–5] Due to the generally slower propagation velocities involved, elastic wave approaches for diagnostics suffer from much poorer resolution as compared to what is achievable using electromagnetics. However, the longer time scales, greater depth of penetration in various media, and non-irradiative and cost-effective transduction make elastic waves attractive for sensing and device applications.

Phononics has made impressive contributions in recent years, including fundamental advances for sensing, imaging, control, vibration damping, cloaking and wavefront manipulation, and exciting phenomena such as topological and edge states.[6–20] The prospect of phononic crystal and metamaterial based novel media that can perform sensing, imaging, and computing with major advances over conventional approaches is exciting. However, in order to truly unveil an era of phononics rivaling those of electronics and photonics, we would need, like in those counterparts, a true source of single (and later, entangled) phonons, and this has not yet been experimentally realized anywhere in the world. The first observation of quantum states of vibration was made less than a decade ago through cooling to the ground state.[21] Most proposals for phonon sources until date remain theoretical.

With the world racing in the quest for "quantum supremacy," increasingly, however, many researchers have come to view quantum phononics as a natural base for advanced computing processes.[22,23] This is especially germane in view of the increasingly escalating demand for cooling in current sensing and computing architectures that rely on electronics or, more recently, photonics. Indeed, prohibitive costs of cooling may eventually put a hold on "Moore's law" expansion of device capabilities.[24,25] Quantum phononics also provides the opportunity to achieve low-noise (sub-Poissonian, where number distribution is such that the variance is less than the mean) imaging at very high frequencies, harnessing phenomena such as entanglement[26] and squeezed states,

yielding potentially unrivalled precision in non-invasive materials diagnostics.

With multiple unique properties of engineering interest and scalability, phononics offers a radically new route for quantum computing.[25] With the ability to be maintained for a long time before being eventually damped and to interact with a wide range of quantum systems such as electric, magnetic, and optical, phonons are promising candidates for quantum devices.[22–25,27,28] Photons, though currently the primary candidates for quantum devices, require sophisticated setups, making practical commercial scalability challenging.[29] With a natural ability to harness waste heat and vibration, phononic computing and sensing would also link back to the earliest era of computing and devices that involved macro-scale mechanical elements such as valves and gears.

Systems with discreet frequency-selective energy levels could be thought of as analogs of or to imitate the behavior of atoms, with non-integer excitations causing release of particles (e.g., electrons in real atoms). However, in real atoms that host fermionic (or physical/matter) particles such as electrons, multiple particles do not co-exist in the same quantum state. Thus, a source of (bosonic) quasi-particles such as single phonons must have "antibunching," a quantum phenomenon whereby only a single quasi-particle can exist in a given system,[30,31] and additional energy input to the system results in the release of excess particles (phonon or photon emission).

Phonon blockade, analogous to "photon blockade" for photons and Coulomb blockade for electrons, is typically used to affect antibunching. Initial research in this direction, deriving from similar concepts in photonics, explored the use of non-linear oscillators (in particular, micro-nanoscale beams) to achieve antibunching.[32–38] Such a "conventional" phonon blockade involves a strong non-linearity in the mechanical resonator to achieve antibunching.[39–42] However, the typical intrinsic nonlinearity of most micro/nanomechanical resonators is usually very weak,[43–48] which makes this method difficult to implement, in practice. Unconventional phonon blockade (UPB) solves this by enabling antibunching even with a weak non-linearity in a system of coupled mechanical oscillators.[49]

However, the devices proposed so far require state-of-the-art nanofabrication and refrigeration capabilities, making them impracticable for scalable practical deployment. These requirements, of manufacturability and temperature control, are stringent because unlike in their photonic counterparts, because of the underlying processes, the thermal phonon number is not negligible in mechanical resonators and therefore significantly influences the phonon blockade even at temperatures of the order of several milli-Kelvins.[38,49,50] Moreover, concepts such as those in Ref. 49 are not hermetically sealable, and thus, fabrication in phononic devices is a challenge.

To address the need for accessing antibunching phenomenon in larger, hotter systems, we propose here a compact, hermetically sealable device, with the goal of achieving optimal parameters of near-micrometer dimensions and near-Kelvin operation. In what follows, first the proposed model is described, along with equations governing the system. The results on antibunching obtainable using the proposed system and optimization of parameters to achieve this at higher dimensions and temperatures are then discussed. The paper concludes with directions for further work.

II. MODEL: COMPACT, HERMETICALLY SEALABLE DEVICE TO REALIZE ANTI-BUNCHING IN PHONONS

As shown in Fig. 1, the proposed system consists of two Coulomb-coupled, circumferentially clamped, identical circular membranes under pre-tension(s). The first membrane (referred to as resonator 1) is a linear resonator coherently driven by an external force, while the other (resonator 2) contains a weak Duffing non-linearity without driving. The casing is rigid and fixed in space to prevent boundary movement. This system is hermetically sealable and hence yields a convenient route for large-scale device fabrication and integration within circuits.

The driving frequency, material properties of the membranes, quantity of charge, separation, and pre-tension imparted are thus the tunable parameters for the device. We assume that resonator 1 is linear and is harmonically driven externally by a force of amplitude F and frequency ω_d. Based on analysis for other coupled resonator systems reported (see, for example, Refs. 29 and 49), the Hamiltonian for this system can be written as (assuming terms to be divided by $\hbar$)

$$
\begin{aligned}
H = {} & \omega_1 \hat{b}_1^\dagger \hat{b}_1 + \omega_2 \hat{b}_2^\dagger \hat{b}_2 + J(\hat{b}_1^\dagger + \hat{b}_1)(\hat{b}_2^\dagger + \hat{b}_2) \\
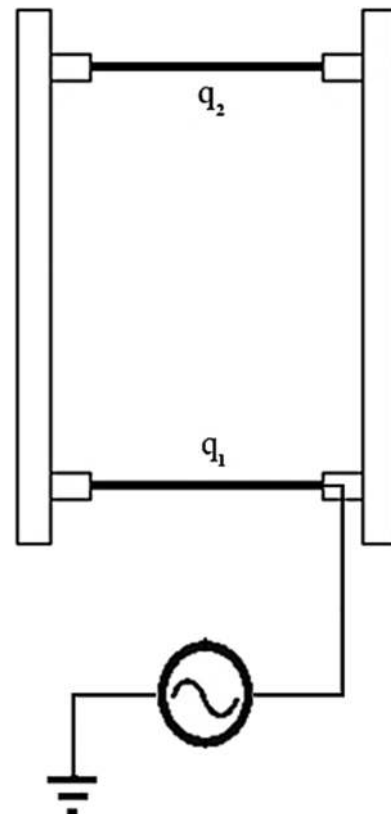& + F(\hat{b}_1^\dagger e^{i\omega_d t} + \hat{b}_1 e^{-i\omega_d t}) + U(\hat{b}_2^\dagger + \hat{b}_2)^4,
\end{aligned}
\tag{1}
$$

FIG. 1. Schematic of the proposed device concept to achieve phonon antibunching.

where $\hat{b}_j \left(\hat{b}_j^\dagger \right)$ is the annihilation (creation) operator for the phonon mode of the jth mechanical resonator with resonance frequency ω_j and decay rate $\gamma_j (j = 1, 2)$. The coupling strength between the two mechanical resonators is denoted by J, while U is the nonlinearity of mechanical resonator 2.

Without loss of generality, in the following, we make the simplifying assumption that the mechanical resonators are identical (i.e., $\omega_1 = \omega_2 = \omega_0$; $\gamma_1 = \gamma_2 = \gamma$) and that the coupling strength J and the nonlinearity U are much smaller compared to the resonance frequency ω_d: $J \ll \omega_0$; $U \ll \omega_0$. The pre-tension and the material of the membranes dictate the resonance frequency, while charge and separation parameters control the coupling strength J through the following relation (see the supplementary material for derivation):

$$J = -\frac{1}{2} \frac{d^2 \left(U_e(z) \right)}{dz^2} \sqrt{\frac{1}{m_1 m_2 \omega_0^2}}, \quad (2)$$

where m_1, m_2 are the masses and ω_0 is the frequency of resonators.

In order to evaluate the double derivative in Eq. (2), we write an expression for the potential energy U_e between two uniformly charged disks of the same radius and separation of z[51] as

$$U_e(z) = \frac{4 k_e Q_1 Q_2}{R} \left(-\frac{a}{2} + \frac{a}{6\pi} \times \left[\left(4 - a^2 \right) E\left(-\frac{4}{a^2} \right) \right. \right.$$
$$\left. \left. + \left(4 + a^2 \right) K\left(-\frac{4}{a^2} \right) \right] \right), \quad (3)$$

where Q_1 and Q_2 are the charges, $a = |z|/R$, and for real values of an argument μ, $K(\mu)$ and $E(\mu)$ are complete elliptic integrals of the first and second kind, respectively.

Equations (1) and (2) help to find and tune the value of J for any given values of charge and separation. Neglecting the anti-rotating wave terms next, we can rewrite the Hamiltonian as

$$H = \Delta \left(\hat{b}_1^\dagger \hat{b}_1 + \hat{b}_2^\dagger \hat{b}_2 \right) + J \left(\hat{b}_1^\dagger \hat{b}_2 + \hat{b}_2^\dagger \hat{b}_1 \right) + F \left(\hat{b}_1^\dagger + \hat{b}_1 \right) + U \hat{b}_2^{2\dagger} \hat{b}_2^2, \quad (4)$$

where $\Delta = \omega_0 - \omega_d$ is the detuning of ω_0 from the driving frequency ω_d.

Equation (4) gives the Hamiltonian for externally driven coupled nonlinear mechanical resonators with dissipation and is similar to the relations in the optical (photonic) context.[52] However, unlike in photonics, temperature plays a major role here due to the lower energy of individual phonons. If we include a temperature factor again assuming it to be the same for both the resonators, and neglect dephasing (since this is typically much smaller than decay[53]), the Liouville–von Neumann master equation for the density matrix yields

$$\frac{d\hat{\rho}}{dt} = \hat{L}\hat{\rho} = -i[H, \hat{\rho}] + \sum_{n=1,2} \frac{\gamma}{2} \left\{ (n_{th} + 1) D\left[\hat{b}_n \right] \hat{\rho} + n_{th} D\left[\hat{b}_n^\dagger \right] \hat{\rho} \right\}, \quad (5)$$

where the Lindblad operator $D\left[\hat{A} \right] \hat{\rho} = 2\hat{A}\hat{\rho}\hat{A}^\dagger - \hat{A}^\dagger \hat{A}\hat{\rho} - \hat{\rho}\hat{A}^\dagger \hat{A}$ and $n_{th} = \left(\exp\left(\frac{T_0}{T} \right) - 1 \right)^{-1}$ is the average phonon number of the mechanical resonators at the temperature T with $T_0 = \hbar\omega/K_B$.

Phonon states for mechanical resonator 1 are given by the second-order correlation function as follows:

$$g^{(2)}(0) = \frac{Tr\left(\hat{b}_1^\dagger \hat{b}_1^\dagger \hat{b}_1 \hat{b}_1 \hat{\rho}_{ss} \right)}{Tr\left(\hat{b}_1^\dagger \hat{b}_1 \hat{\rho}_{ss} \right)^2}, \quad (6)$$

where the density matrix

$$\hat{\rho} = \sum_{m,n=0}^{N} \rho_{mn,m'n'} |mn\rangle\langle m'n'| \quad (7)$$

is evaluated based on $|mn\rangle$, m and n denoting the phonon number in mechanical modes 1 and 2, respectively, and $\hat{\rho}_{ss}$ is the steady-state density matrix obtained by setting $\frac{d\hat{\rho}}{dt} = 0$ in Eq. (5), yielding an eigenvalue problem that can be numerically solved using the approach in Ref. 54. In the numerical calculations reported here, $m = n = 10$, large enough to ensure convergence.

III. RESULTS

It has been shown that 0.04 T_0 (where $T_0 = h\omega_0/2\pi K_B$) is a suitable system temperature for phonon antibunching.[49] As the temperature is pushed higher, antibunching fades. This puts an upper bound on our system temperature. Given that the design in Ref. 55 conceived a compact 3 mK refrigeration in the latter part of 1980s, with modern day machinery, this threshold of cooling capacity should be feasible: hence, this has been chosen as the lower bound for our system temperature. We thus take

$$3 \, \text{mK} \leq T_{sys} \leq 0.04 T_0. \quad (8)$$

The smallest system dimension (z_{sys}) and the system temperature (T_{sys}) are the two objectives to be maximized. We take the largest allowed value for system temperature, i.e., ($T_{sys} = 0.04 T_0$), and express T_0 in terms of system's natural frequency as

$$T_{sys} = f_{sys} \times \beta; \beta = \frac{h}{K_B} = \left(1.9196 \times 10^{-12} \, \text{K s} \right). \quad (9)$$

f_{sys} can be related to (z_{sys}) using structural mechanics of the resonator.[56] Using (9), f_{sys} can be written in terms of T_{sys} giving us relations between T_{sys} and Z_{sys}. Through simple algebraic manipulation, it is found that for all the geometries studied, trade-off curves between T_{sys} and Z_{sys} take the form

$$T_{sys} \times Z_{sys} = P. \quad (10)$$

This means that for a given value of T_{sys}, maximizing Z_{sys} would mean maximizing P and vice versa. The structural mechanics expression of P depends on the geometric configuration and material factors pertaining to the resonator design, which when grouped and re-written gives

$$P = \alpha_g \times P_a \times P_g \times P_m \times \beta. \quad (11)$$

Here, α_g, P_a, and P_g are dimensionless and configuration (geometry) dependent. α_g is a numerical value dependent on the configuration chosen, and P_a, P_g, and P_m are performance parameters that can be tuned by changing the aspect ratio, cross-sectional geometry, and material properties, respectively. P_m and P have dimensions of $[L][T^{-1}]$ and $[L][K]$, respectively.

TABLE I. Performance metrics and their optimal values for different geometries.

Resonator geometry	α_g	P_a	P_g	P_m	P_a optimal	P_g optimal	P(m-K) optimal
Circular membrane	$\frac{2.405}{2\pi}$	$\frac{t}{R}$	$\frac{1}{1}$	$\sqrt{\sigma/\rho}$	0.2	1	9.47×10^{-10}
Hollow rectangular beam	$\frac{22.373}{2\pi}$	$\frac{H^2}{L^2}$	$\frac{1}{\sqrt{12}}\sqrt{\frac{1-c^3 d}{1-cd}}$	$\sqrt{E/\rho}$	0.01	0.371	4.72×10^{-10}
Hollow circular beam	$\frac{22.373}{2\pi}$	$\frac{D^2}{L^2}$	$\frac{1}{\sqrt{16}}\sqrt{1+r^2}$	$\sqrt{E/\rho}$	0.01	0.320	4.06×10^{-10}
Solid rectangular beam	$\frac{22.373}{2\pi}$	$\frac{H^2}{L^2}$	$\frac{1}{\sqrt{12}}$	$\sqrt{E/\rho}$	0.01	0.288	3.66×10^{-10}
Solid circular beam	$\frac{22.373}{2\pi}$	$\frac{D^2}{L^2}$	$\frac{1}{\sqrt{16}}$	$\sqrt{E/\rho}$	0.01	0.250	3.17×10^{-10}
I-beam	$\frac{22.373}{2\pi}$	$\frac{H^2}{L^2}$	$\frac{1}{\sqrt{12}}\sqrt{\frac{1-c^3+c^3 d}{1-c+cd}}$	$\sqrt{E/\rho}$	0.01	0.371	4.72×10^{-10}

Once the geometry configuration is chosen, α_g becomes determined and the overall problem can be split into three sub-problems pertaining to optimization of each of the individual performance metrics P_a, P_g, and P_m. For ideally compliant structures, the material performance metric P_m becomes the square root of specific strength $\sqrt{\sigma/\rho}$, and for ideally elastic structures, it becomes the square root of specific stiffness $\sqrt{E/\rho}$, where σ, ρ, and E are of the material chosen for the linear resonator.

Here, the compliant structure studied is the circumferentially clamped isotropic circular membrane, and elastic structures studied are rectangular cross-sectional beams (both solid and hollow), circular cross-sectional beams (both solid and hollow), and I-beams. Expressions for α_g, P_a, P_g, and P_m along with their optimal values for these are listed in Table I. The fraction of the material removed radius-wise, height-wise, and width-wise are r, c, and d, respectively (evaluation performed at $r = 0.8$, $c = 0.75$, and $d = 0.8$). With regards to material metric P_m, it is found that in circular membranes, graphene optimizes the value of P_m to 7900 m/s,[57] while in beams, diamond optimizes the value of P_m to 18 600 m/s.[58] The maximal

value of t/R is 0.2 (for the thin disk approximation) and H/L and D/L is 0.1 (for the slender beam approximation).

IV. DISCUSSION

Trade-off curves between T_{sys} and Z_{sys} are plotted in Fig. 2, while the results of optimizations of Z_{sys} and T_{sys} values pertaining to each of the configurations are listed in Tables II and III.

For the circular membrane, the J value is tunable and the F value is adjusted externally. Parametric sensitivity analysis is carried out to check the effects of non-linearity U and coupling strength J, both of which are known to have a crucial effect on the second order correlation function $g^{(2)}(0)$, which is a measure of the antibunching in the system. The resulting variations are plotted in Figs. 3 and 4, respectively. The results indicate that for $J^* = 110$, $U^* = 3 \times 10^{-5}$, $F^* = 10$, and $\Delta^* = 0.29$; $g^{(2)}(0) \ll 1$, which implies strong anti-bunching. Note that $J^* = J/\gamma$; likewise, U^*, F^*, and Δ^* are also non-dimensional analogs generated by dividing with the decay rate (γ).
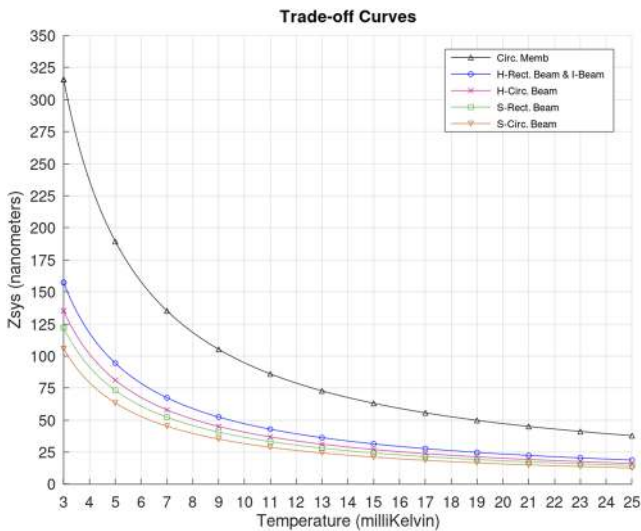

FIG. 2. Trade-off curves between T_{sys} and Z_{sys} for different geometries as discussed in Tables II and III.

TABLE II. Z_{sys} values for different configurations at different T_{sys} values.

Configuration	Z_{sys} for 3 mK	Z_{sys} for 25 mK
Circular membrane	315 nm	37.9 nm
H-rectangular beam	157 nm	18.8 nm
H-circular beam	135 nm	16.2 nm
S-rectangular beam	122 nm	14.6 nm
S-circular beam	105 nm	12.7 nm
I-beam	157 nm	18.8 nm

TABLE III. T_{sys} values for different configurations at different Z_{sys} values.

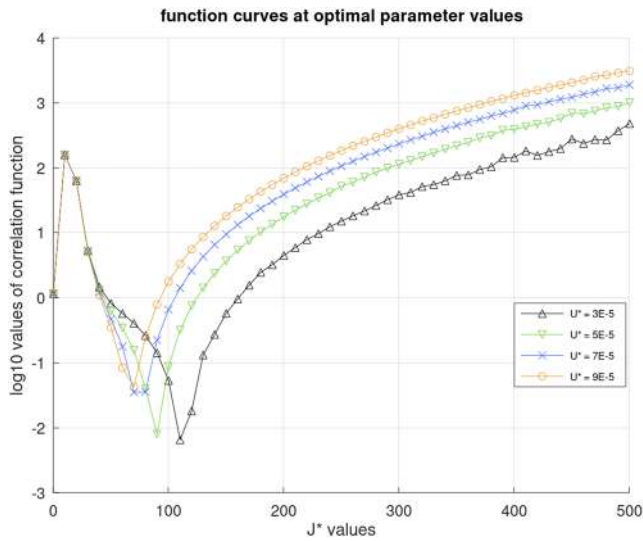| Configuration	T_{sys} for 0.1 μm	Z_{sys} for 25 mK
Circular membrane	9.47 mK	37.9 nm
H-rectangular beam	4.72 mK	18.8 nm
H-circular beam	4.06 mK	16.2 nm
S-rectangular beam	3.66 mK	14.6 nm
S-circular beam	3.17 mK	12.7 nm
I-beam	4.72 mK	18.8 nm

FIG. 3. Variation of $g^{(2)}(0)$ with the coupling strength. Here, $F = 10\gamma$ and $\Delta = 0.29\gamma$.

From the above results, the effect of non-linearity U on $g^{(2)}(0)$ can be seen in terms of two behaviors. First, increasing the value of coupling strength J allows the devices to work at lesser non-linearity, and the strength of antibunching reduces but still remains sufficiently strong [$g^2(0) \ll 0.1$]. Second, we note that the antibunching performance of different configurations follows similar curves consisting of a dip followed by a tail of increasing $g^2(0)$ values. We also note here that in Ref. 59, deposition of graphene onto a silicon nitride substrate is shown as a feasible method of inducing and
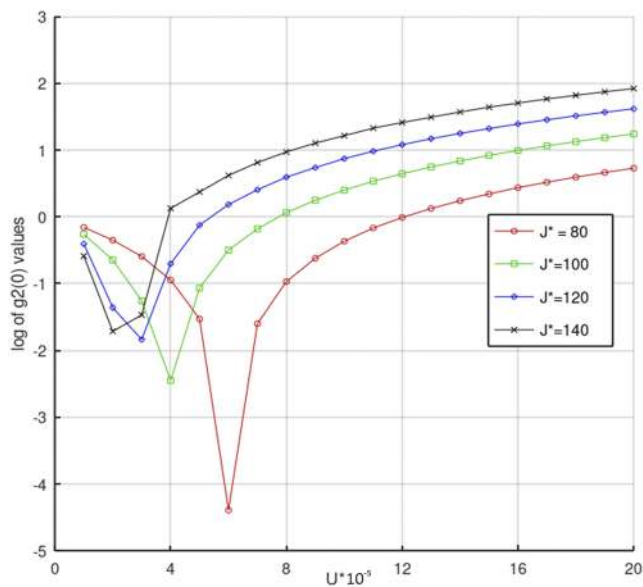

FIG. 4. Variation of $g^{(2)}(0)$ with non-linearity. Here, $F = 10\gamma$ and $\Delta = 0.29\gamma$.

finely controlling the non-linearity of mechanical resonators (see the supplementary material for a discussion of how we may achieve the low non-linearities in the range of results reported here, using the approach of Ref. 59). Together with our findings reported here, such methods that can help modify the non-linearity without changing dimensions can be used to exert control over the strength of antibunching.

V. CONCLUSIONS AND FURTHER WORK

This paper proposed and studied a novel design for a hermetically sealable device, consisting of charged linear and nonlinear membranes driven in the gigahertz range in vacuum setting, as a source of antibunched single phonons. Constraints for effecting phonon antibunching were found using the stationary Liouville–von Neumann master equation. Using analytical calculations and material and geometry optimization, we showed that the sizes of the proposed system can be upscaled to the near-micrometer range in a trade-off with the system operating temperature. We argue that if the material properties are also optimized and the hollow rectangular beam (with central 75% height-wise and 80% width-wise material removed) is used, device dimensions can be pushed up to 157 nm using diamond. Graphene helps to scale up the dimensions further to 315 nm at 3 mK. This work contributes toward making phonon-based quantum devices more accessible and scalable. Furthermore, for all the geometries considered, the results show that the temperature requirement at 0.1 μm scale is greater than 3 mK hence above the set lower-bound. Further and ongoing work at our group is studying the development of density of states from the Hamiltonian, exploring the origins of antibunching in nanomechanical resonator systems. Approaches to fabricate and test the device proposed here are also being initiated.

SUPPLEMENTARY MATERIAL

The supplementary material provides a detailed derivation of the coupling strength J, as given in Eq. (2), based on the procedure in Ref. 29 and also describes how we may achieve non-linearities U in the range of values of interest to this work through the approach in Ref. 59.

DATA AVAILABILITY

The data that support the findings of this study are available from the corresponding author upon reasonable request.

REFERENCES

[1] M. P. Marder, *Condensed Matter Physics*, 2nd ed. (John Wiley & Sons, Hoboken, NJ, 2010).

[2] M. Maldovan, "Sound and heat revolutions in phononics," Nature **503**(7475), 209–217 (2013).

[3] S. Periyannan, K. Balasubramaniam, and P. Rajagopal, "Re-configurable multi-level temperature sensing by ultrasonic 'spring-like' helical waveguide," J. Appl. Phys. **119**(14), 144502 (2016).

[4] D. R. Thakare, A. Abid, D. Pereira, J. Fernandes, P. Belanger, and P. Rajagopal, "Semi-analytical finite-element modeling approach for guided wave assessment of mechanical degradation in bones," Int. Biomech. **4**(1), 17–27 (2017).

[5]R. S. Panda, P. Rajagopal, and K. Balasubramaniam, "Rapid guided wave inspection of complex stiffened composite structural components using non-contact air-coupled ultrasound," Compos. Struct. **206**, 247–260 (2018).

[6]J. B. Pendry, D. Schurig, and D. R. Smith, "Controlling electromagnetic fields," Science **312**(5781), 1780–1782 (2006).

[7]*Phononic Crystals: Fundamentals and Applications*, edited by A. Khelif and A. Abidi (Springer Science + Business Media, New York, 2016), ISBN: 978-1-4614-9392-1.

[8]S. A. R. Kuchibhatla and P. Rajagopal, "A transformation elasticity-based device for wavefront manipulation," NDT & E Int. **102**, 304–310 (2019).

[9]R. Lucklum, M. Ke, and M. Zubtsov, "Two-dimensional phononic crystal sensor based on a cavity mode," Sens. Actuators, B **171-172**, 271–277 (2012).

[10]S. Mohammadi, A. Khelif, and A. Adibi, "Future prospects of phononic crystals and phononic metamaterials," in *Phononic Crystals* (Springer, New York, 2016), pp. 239–245.

[11]Y. Pennec, Y. Jin, and B. Djafari-Rouhani, "Phononic and photonic crystals for sensing applications," Adv. Appl. Mech. **52**, 105–145 (2019).

[12]J. Bonhomme, M. Oudich, B. Djafari-Rouhani, F. Sarry, Y. Pennec, B. Bonello, D. Beyssen, and P. G. Charette, "Love waves dispersion by phononic pillars for nano-particle mass sensing," Appl. Phys. Lett. **114**(1), 013501 (2019).

[13]K. K. Amireddy, K. Balasubramaniam, and P. Rajagopal, "Holey-structured metamaterial lens for subwavelength resolution in ultrasonic characterization of metallic components," Appl. Phys. Lett. **108**, 224101 (2016).

[14]K. K. Amireddy, K. Balasubramaniam, and P. Rajagopal, "Deep subwavelength ultrasonic imaging using optimized holey structured metamaterials," Sci. Rep. **7**, 7777 (2017).

[15]K. K. Amireddy, K. Balasubramaniam, and P. Rajagopal, "Porous metamaterials for deep sub-wavelength ultrasonic imaging," Appl. Phys. Lett. **113**(12), 124102 (2018).

[16]M. S. Syed Akbar Ali, K. K. Amireddy, K. Balasubramaniam, and P. Rajagopal, "Characterization of deep sub-wavelength sized horizontal cracks using holey-structured metamaterials," Trans. Indian Inst. Metals **72**(11), 2917–2921 (2019).

[17]C. T. Manjunath and P. Rajagopal, "Lensing in the ultrasonic domain using negative refraction induced by material contrast," Sci. Rep. **9**, 6368 (2019).

[18]M. Maldovan, "Phonon wave interference and thermal bandgap materials," Nat. Mater. **14**(7), 667–674 (2015).

[19]A. A. Zul Karnain, S. A. R. Kuchibhatla, T. Thomas, and P. Rajagopal, "Semiconductor based thermal wave crystals," ISSS J. Micro Smart Syst. **9**, 181 (2020).

[20]S. A. Cummer, J. Christensen, and A. Alù, "Controlling sound with acoustic metamaterials," Nat. Rev. Mater. **1**(3), 16001 (2016).

[21]A. D. O'Connell, M. Hofheinz, M. Ansmann, R. C. Bialczak, M. Lenander, E. Lucero, M. Neeley, D. Sank, H. Wang, M. Weides, J. Wenner, J. M. Martinis, and A. N. Cleland, "Quantum ground state and single-phonon control of a mechanical resonator," Nature **464**(7289), 697 (2010).

[22]K. Stannigel, P. Komar, S. J. M. Habraken, S. D. Bennett, M. D. Lukin, P. Zoller, and P. Rabl, "Optomechanical quantum information processing with photons and phonons," Phys. Rev. Lett. **109**, 013603 (2012).

[23]S. Rips and M. J. Hartmann, "Quantum information processing with nanomechanical qubits," Phys. Rev. Lett. **110**, 120503 (2013); Erratum **111**, 049905 (2013).

[24]C. M. Reinke and I. El-Kady, "Phonon-based scalable platform for chip-scale quantum computing," AIP Adv. **6**(12), 122002 (2016).

[25]S. R. Sklan, "Splash, pop, sizzle: Information processing with phononic computing," AIP Adv. **5**(5), 053302 (2015).

[26]R. Demkowicz-Dobrzański, J. Kołodyński, and M. Guţă, "The elusive Heisenberg limit in quantum-enhanced metrology," Nat. Commun. **3**, 1063 (2012).

[27]S. J. M. Habraken, K. Stannigel, M. D. Lukin, P. Zoller, and P. Rabl, "Continuous mode cooling and phonon routers for phononic quantum networks," New J. Phys. **14**, 115004 (2012).

[28]M. V. Gustafsson, T. Aref, A. F. Kockum, M. K. Ekstrom, G. Johansson, and P. Delsing, "Propagating phonons coupled to an artificial atom," Science **346**, 207 (2014).

[29]B. Sarma and A. K. Sarma, "Tunable phonon blockade in weakly nonlinear coupled mechanical resonators via Coulomb interaction," Sci. Rep. **8**(1), 14583 (2018).

[30]Y. X. Liu, A. Miranowicz, Y. B. Gao, J. Bajer, C. P. Sun, and F. Nori, "Qubit-induced phonon blockade as a signature of quantum behavior in nanomechanical resonators," Phys. Rev. A **82**, 032101 (2010).

[31]A. Imamoglu, H. Schmidt, G. Woods, and M. Deutsch, "Strongly interacting photons in a nonlinear cavity," Phys. Rev. Lett. **79**, 1467 (1997).

[32]M. Eichenfield, J. Chan, R. M. Camacho, K. J. Vahala, and O. Painter, "Optomechanical crystals," Nature **462**(7269), 78 (2009).

[33]X. Y. Lü, W. M. Zhang, S. Ashhab, Y. Wu, and F. Nori, "Quantum-criticality-induced strong Kerr nonlinearities in optomechanical systems," Sci. Rep. **3**, 2943 (2013).

[34]M. Aspelmeyer, T. J. Kippenberg, and F. Marquardt, "Cavity optomechanics," Rev. Mod. Phys. **86**(4), 1391 (2014).

[35]I. Söllner, L. Midolo, and P. Lodahl, "Deterministic single-phonon source triggered by a single photon," Phys. Rev. Lett. **116**(23), 234301 (2016).

[36]A. Barasiński, W. Leoński, and T. Sowiński, "Ground-state entanglement of spin-1 bosons undergoing superexchange interactions in optical superlattices," JOSA B **31**(8), 1845–1852 (2014).

[37]W. Xiong, D. Y. Jin, J. Jing, C. H. Lam, and J. Q. You, "Controllable coupling between a nanomechanical resonator and a coplanar-waveguide resonator via a superconducting flux qubit," Phys. Rev. A **92**(3), 032318 (2015).

[38]X. Wang, A. Miranowicz, H. R. Li, and F. Nori, "Method for observing robust and tunable phonon blockade in a nanomechanical resonator coupled to a charge qubit," Phys. Rev. A **93**(6), 063861 (2016).

[39]N. Didier, S. Pugnetti, Y. M. Blanter, and R. Fazio, "Detecting phonon blockade with photons," Phys. Rev. B **84**, 054503 (2011).

[40]A. Miranowicz, J. Bajer, N. Lambert, Y. X. Liu, and F. Nori, "Tunable multiphonon blockade in coupled nanomechanical resonators," Phys. Rev. A **93**, 013808 (2016).

[41]X. W. Xu, A. X. Chen, and Y. X. Liu, "Phonon blockade in a nanomechanical resonator resonantly coupled to a qubit," Phys. Rev. A **94**, 063853 (2016).

[42]H. Seok and E. M. Wright, "Antibunching in an optomechanical oscillator," Phys. Rev. A **95**, 053844 (2017).

[43]G.-W. Deng, D. Zhu, X.-H. Wang, C.-L. Zou, J.-T. Wang, H.-O. Li, G. Cao, D. Liu, Y. Li, M. Xiao, G.-C. Guo, K.-L. Jiang, X.-C. Dai, and G.-P. Guo, "Strongly coupled nanotube electromechanical resonators," Nano Lett. **16**, 5456 (2016).

[44]A. N. Cleland and M. L. Roukes, "Noise processes in nanomechanical resonators," J. Appl. Phys. **92**, 2758 (2002).

[45]T. Veijola and T. Mattila, "Modeling of nonlinear micromechanical resonators and their simulation with the harmonic-balance method," Int. J. RF Microwave Comput. Aided Eng. **11**, 310–321 (2001).

[46]V. Peano and M. Thorwart, "Nonlinear response of a driven vibrating nanobeam in the quantum regime," New J. Phys. **8**, 21 (2006).

[47]E. Babourina-Brooks, A. Doherty, and G. J. Milburn, "Quantum noise in a nanomechanical duffing resonator," New J. Phys. **10**, 105020 (2008).

[48]I. Katz, A. Retzker, R. Straub, and R. Lifshitz, "Signatures for a classical to quantum transition of a driven nonlinear nanomechanical resonator," Phys. Rev. Lett. **99**, 040404 (2007).

[49]S. Guan, W. P. Bowen, C. Liu, and Z. Duan, "Phonon antibunching effect in coupled nonlinear micro/nanomechanical resonator at finite temperature," Europhys. Lett. **119**(5), 58001 (2017).

[50]S. Barzanjeh and D. Vitali, "Phonon Josephson junction with nanomechanical resonators," Phys. Rev. A **93**(3), 033846 (2016).

[51]O. Ciftja, "Electrostatic interaction energy between two coaxial parallel uniformly charged disks," Results Phys. **15**, 102684 (2019).

[52]M. Bamba, A. Imamoglu, I. Carusotto, and C. Ciuti, "Origin of strong photon antibunching in weakly nonlinear photonic molecules," Phys. Rev. A **83**, 021802 (2011).

[53]T. Hahn, D. Groll, T. Kuhn, and D. Wigger, "Influence of excited state decay and dephasing on phonon quantum state preparation," Phys. Rev. B **100**(2), 024306 (2019).

[54]V. Savona, "Unconventional photon blockade in coupled optomechanical systems," arXiv:1302.5937 (2013).

[55]A. M. Guénault, D. J. Hayward, I. E. Miller, T. R. Nichols, and G. R. Pickett, "A compact high-circulation 3 mK dilution refrigerator with HCP vertical heat exchangers," Jpn. J. Appl. Phys., Part 1 **26**, 1725 (1987).

[56]R. D. Blevins, *Formulas for Dynamics, Acoustics and Vibration* (John Wiley & Sons, 2015), ISBN: 978-1-119-03811-5.

[57]C. Lee, X. Wei, J. W. Kysar, and J. Hone, "Measurement of the elastic properties and intrinsic strength of monolayer graphene," Science **321**(5887), 385–388 (2008).

[58]K. E. Spear and J. P. Dismukes, *Synthetic Diamond: Emerging CVD Science and Technology* (Wiley, NY, 1994), p. 315.

[59]R. Singh, A. Sarkar, C. Guria, R. J. T. Nicholl, S. Chakraborty, K. I. Bolotin, and S. Ghosh, "Giant tunable mechanical nonlinearity in graphene-silicon Nitride hybrid resonator," Nano Lett. **20**(6), 4659–4666 (2020).